Annealing novel nucleobase-lipids with oligonucleotides or plasmid DNA based on H-bonding or π-π interaction

Ma, Yuan; Zhu, Yuejie; Wang, Chao; Pan, Delin; Liu, Shuang; Yang, Mengyi; Xiao, Zhangping; Yang, Xiantao; Zhao, Wenting; Zhou, Xinyang

Published in:
Biomaterials

DOI:
10.1016/j.biomaterials.2018.06.012

Publication date:
2018

Biomaterials 178 (2018) 147–157

Contents lists available at ScienceDirect

Biomaterials

journal homepage: www.elsevier.com/locate/biomaterials

Annealing novel nucleobase-lipids with oligonucleotides or plasmid DNA based on H-bonding or π-π interaction: Assemblies and transfections

Yuan Ma [1], Yuejie Zhu [1], Chao Wang, Delin Pan, Shuang Liu, Mengyi Yang, Zhangping Xiao, Xiantao Yang, Wenting Zhao, Xinyang Zhou, Yiding Li, Yufei Pan, Jing Sun, Shuhe Wang, Zhu Guan, Lihe Zhang, Zhenjun Yang*

State Key Laboratory of Natural and Biomimetic Drugs, School of Pharmaceutical Sciences, Peking University, No.38 Xueyuan Road, Haidian District, Beijing 100191, China

ARTICLE INFO

Article history:
Received 16 April 2018
Received in revised form
7 June 2018
Accepted 9 June 2018
Available online 14 June 2018

Keywords:
Gene delivery
Nucleobase-lipid
Self-assembly
Oligonucleotide
Plasmid DNA

ABSTRACT

Lipid derivatives of nucleoside analogs have been highlighted for their potential for effective gene delivery. A novel class of nucleobase-lipids are rationally designed and readily synthesized, comprising thymine/cytosine, an ester/amide linker and an oleyl lipid. The diversity of four nucleobase-lipids termed DXBAs (DOTA, DNTA, DOCA and DNCA) is investigated. Besides, DNCA is demonstrated to be an effective neutral transfection material for nucleic acid delivery, which enbles to bind to oligonucleotides via H-bonding and π-π stacking with reduced toxicity *in vitro* and *in vivo*. Several kinds of nucleic acid drugs including aptamer, ssRNA, antisense oligonucleotide, and plasmid DNAs can be delivered by DXBAs, especially DNCA. In particular, G4-aptamer AS1411 encapsulated by DNCA exhibits cellular uptake enhancement, lysosome degradation reduction, cell apoptosis promotion, cell cycle phase alteration *in vitro* and duration prolongation *in vivo*, resulting in significant anti-proliferative activity. Our results demonstrate that DNCA is a promising transfection agent for G4-aptamers and exhibites bright application prospects in the permeation improvement of single-stranded oligonucleotides or plasmid DNAs.

1. Introduction

In past decades, nucleic acid drugs have gained significant attention owing to tremendous potentials for the treatment of inherited diseases [1]. However, efficient and biocompatible delivery of nucleic acids remains great challenging [2]. Many classes of organic or inorganic materials have been developed as nucleic acids carrier for overcoming their transmembrane difficulty. The drug vehicles mainly include viral-capsids, lipids, cyclodextrin, peptides, mesoporous silica or gold nanoparticles [3], in which the first two are most widely used in clinical research for gene therapy [4,5]. Compared with viral vectors, lipids are easy to fabricate with lower immunogenicity [6]. Cationic lipids can pack nucleic acids into nanoparticles via electrostatic interaction [7], and *Patisiran*, comprising siRNA and cationic lipid (1,2-dilinoleyloxy-3-dimethylaminopropane, DLinDMA)-based nanoparticles coated with apolipoprotein E (ApoE), has efficacy in phase 3 clinical trials. However, most of cationic transfection agents are frequently applied *in vitro* [8], because the cytotoxicity and possibility of negatively charged serum proteins binding at physiological pH greatly restrict further applications [9,10]. For now, there have been very few oligonucleotide drugs approved by the FDA, and all of them are alternatively local injection or systemic injection with high dosage for no suitable carrier. For example, a kind of antisense oligonucleotide (*Kynamro*) has usually reached approximately 200 mg week^{-1} [11]. Thus, the effective and low-toxicity delivery of nucleic acids remains key in the application of nucleic acids in the treatment of diseases [12–14]. Nanoparticles with high therapeutic efficacies must be developed urgently [15].

Based on nucleoside-nucleoside interactions, nucleic acids can be used as carrier as well. DNA origami has resulted in construction of suitable scaffolds [16]. Particularly for self-assembled DNA tetrahedrons, they have been widely used as drug delivery systems [17]. Some aromatic compounds may enhance the delivery of

* Corresponding author.
E-mail address: yangzj@bjmu.edu.cn (Z. Yang).
[1] These authors contributed equally.

https://doi.org/10.1016/j.biomaterials.2018.06.012

oligonucleotides [18]. Nucleoside phospholipids [19,20], a covalent combination of molecules carrying lipid moieties with nucleosides, have been recently developed as novel therapeutic agents [21]. In contrast to classical amphiphilic lipids, they possess a highly specialized polar head-group (adenosine, thymidine, cytidine, guanosine, uracil, or their analogs), providing additional hydrogen bonding with complementary nucleobases via Watson-Crick base pairing and π-stacking [22–24], and these lipids can spontaneously self-assemble in water with low toxicity and immunogenicity [25,26]. A number of similar amphiphilic nucleoside-based lipids have then been proposed as drug nanocarriers, especially for gene-based drugs [27]. The nucleotide moiety enhances the transfection efficacy, in which anionic nucleoside-based lipid named diC16-3′-dT [Thymidine 3'-(1,2-dipalmitoyl-*sn*-glycero-3-phosphate)] can be used as a helper lipid for penetrating Hek cells and releasing the plasmid DNA in the presence of DOPE (1,2-dioleoyl-sn-glycero-3-phosphoethanolamine) and Ca^{2+} ions [28]. Additionally, cationic nucleoside-based lipid named TRN [Tosylate salt of 1'-(2′,3′-dioleyl-5′-trimethylammonium-α,β-D-ribofuranosyl)-3-nitropyrrole] significantly enhances siRNA permeation, which exhibites protein knockdown upon mouse fibroblas (NIH 3T3) at N/P ratio of 10 [29]. In our previous works, a novel type of zwitterionic nucleolipids was reasonably designed [30]. Even though the aminonucleoside phospholipids (Fig. 1, DOPAdT) could interact with oligonucleotides and exhibit diverse self-assembly in water, these nucleolipids failed to transfect DNA probably due to the electrostatic repulsion.

To ameliorate the dilemma mentioned above, we present the synthesis and physicochemical characterization of a novel class of nucleobase-lipids, which excludes the phosphate moiety (Fig. 1, DXBAs), aiming to develop an efficient gene-based drug delivery system for further research. These nucleobase-lipids contained the basic structures of thymine/cytosine, glycerinum and oleyl alcohol. Four kinds of nucleobase-lipids were prepared and named DXBAs (DOTA, DNTA, DOCA and DNCA), which were expected to interact with oligonucleotides via Watson-Crick and π-stacking. Our reported synthesis route (provided in detail in the Supplementary Information) illustrated a facile pathway to achieve a wide diversity of these kinds of materials. Moreover, their amphiphilicity and self-assembly were characterized by means of transmission electron microscopy (TEM) and molecular simulation. To illustrate the involved characteristics and interactions, the transfection of nucleic-acid drugs including a G-quadruplex aptamer (AS1411), single-stranded RNAs (122S), an antisense oligonucleotide (G3139) and plasmid DNAs by DXBAs were further investigated with regard to assembly, biological properties and functional mechanisms. It was firstly demonstrated that nucleoside-based lipid (DNCA) participated in the formation of AS1411 G4 structure, which made it become an efficient G4-aptamer carrier as an individual anticancer agent rather than a targeted molecule. The results showed a great potential value of the DNCA lipid for delivering gene-based drugs. Additionally in order to enhance the specificity and encapsulation efficiency for gene drugs delivery, the nucleoside-based lipids could be optimized by conjugation to a targeting molecule or substitution to a universal base, which could strengthen lipid-nucleic acid interaction and exhibit a bright aspect for gene drugs application in further.

2. Materials and methods

2.1. Preparation of oligonucleotides

The unconjugated RNAs were synthesized according to standard phosphonamidite chemistry utilizing an Applied Biosystems 394 DNA Synthesizer (Applied Biosystems, USA), in which peptide-conjugated products were synthesized starting with Pep-CPG (Scheme S1). The crude products were purified by high-performance liquid chromatography (HPLC) using the base ion-exchange column (DionexDNAPac, PA200, 9 × 250 mm). Phase B was 0.02 M Tris-$HClO_4$ with 10% ACN (pH 8.0), and phase A was the same formulation as eluent B with extra 0.4 M $NaClO_4$.

The DNA samples were purchased from Sangon Biotech (China). All oligonucleotides were confirmed by MALDI-TOF MS or ESI MS analyses (Fig. S1). The sequences used were (5′-3′): 122S, r(AAC GCC AUU AUC ACA CUA AAUA); P122S, r(AAC GCC AUUA UCA CAC UAA AUA)-LALLAK; 122A, r(UGG AGU GUG ACA AUG GUG UUUG); P122A, r(UGG AGU GUG ACA AUG GUG UUU G)-LALLAK; 122, 122S/122A duplex; PP122, P122S/P122A duplex; AS1411, d(GGT GGT GGT GGT TGT GGT GGT GG); NC, d(CCT GAC GTC TCT ACG CCG); N-

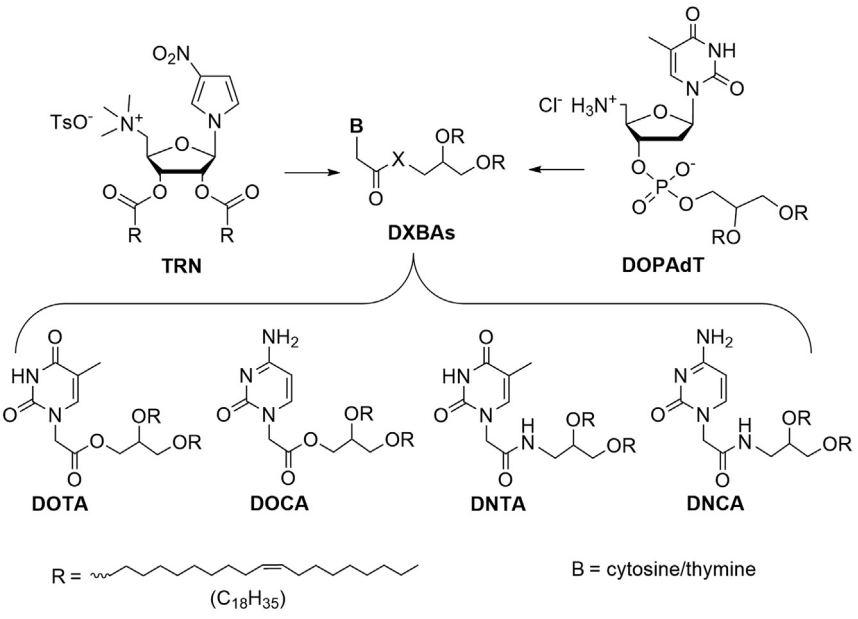

Fig. 1. Chemical structures of nucleobase-lipids.

G3139, d(TCT CCC AGC GTG CGC CAT); and G3139, d(TsCsTs CsCsCs AsGsCs GsTsGs CsGsCs CsAsT). Note: "s" represents PS modification.

2.2. Preparation and characteristics of the lipids

The lipids were synthesized as Schemes S2–S4, and the nanoparticles were performed using the thin-film hydration method [31]. Four types of nucleobase-lipids were individually dissolved in 2 mL of a mixed solution of chloroform and methanol (v/v, 10/1). Solutions were then evaporated to dryness under reduced pressure and dried at room temperature for 30 min in vacuo. Deionized water (1 mL) was added, followed by sonication at 50 °C for 1 h to yield the lipids. Lipid morphologies were observed using a Hitachi H-7650 80-kV transmission electron microscope (TEM), and images were taken by an AMT Camera system. The samples were negatively stained with a sodium phosphotungstate solution (pH 7.2).

2.3. Encapsulation efficiency assay

The concentrations of 6-FAM-labeled RNAs were 2 μM, and the concentrations of the DNAs (AS1411, N-G3139, G3139) were 10 μM. All of the oligonucleotides annealed to the amphiphile at the sampled base ratio. The solution was then mixed with 6 × RNA loading buffer (2 μL, DingGuo, Beijing, China), and the DNAs were made visible using 10,000 × Sybr Gold (5 μL). The samples were then analyzed on 20% polyacrylamide gels at 110 V for 120 min, and intact bands were quantified using ImageLab software.

2.4. Simulation of molecular self-assembly

After the molecule of DNCA was modeled, the minimal energy conformer was calculated using CS Chem3D. The molecular structure was obtained.

In addition, a dissipative particle dynamic (DPD) analysis was performed, which consists of a coarse-grained mesoscopic simulation technique for isothermal complex fluids and soft matter systems with particles that are chosen to be adequate fluid elements and is usually used to simulate the self-assembly of lipids in water. In the model, a series of soft particles, called beads, that represent groups of several atoms or fluids interact with each other. The coarse-grained model of DNTA, DNCA was constructed, respectively. The full molecular models of the fragments of each lipid were constructed in the Discover and Amorphous Cell modules of Materials Studio 5.5 (Accelrys Inc., USA) [32]. After the solubility parameters of the fragments and water were calculated, the Flory–Huggins interaction parameter χ_{ij} of any pair of fragments or of a fragment and water can be obtained by Equation (1):

$$\chi_{ij} = (\delta_i - \delta_j)^2 Vref/RT \quad (1)$$

where i and j are the solubility parameters of a pair of interacting beads, Vref was the average molar volume of two beads—which was calculated using the Discover and Amorphous Cell modules in Materials Studio with the COMPASS force field at 298 K and under atmospheric pressure—R is the gas constant, and T is temperature. The DPD interaction parameters of different beads (α_{ij}) in the lipid/water system were obtained by Equation (2).

$$\alpha_{ij} = 25 + 3.27\chi_{ij} \quad (2)$$

All computational work was performed using Materials Studio 5.5. The simulation system contained the lipid derivatives (e.g., DNCA) and water in a cubic cell of size 30 Å × 30 Å × 30 Å with a periodic boundary condition. The concentration of lipid derivatives was selected as 20% (w/v, lipid derivatives vs. water). The total beads were 33,460 and the spring constant C was chosen as 4.0. To obtain the steady state, 100,000 DPD steps were adopted with a time step of 0.05 ps.

2.5. Cytotoxicity

A CCK-8 assay (cell counting kit-8, Dojindo Laboratories, Kumamoto, Japan) was used to assess the cytotoxicity of DXBA against HeLa cells according to the manufacturer's protocol. Briefly, the cells were seeded onto a 96-well plate at a density of 3000 cells per well and incubated in DMEM at 37 °C under a 5% CO_2/95% air atmosphere overnight. Cells were then incubated with DXBA (65 μM) for another 72 h. Then, 10 μL of CCK-8 assay solution was added to each well of the plate. After incubation for 3 h, the UV absorbance was measured at 450 nm using a Flex Station 3 Benchtop Multi-Mode Microplate Reader (Molecular Devices, CA, USA). The mean cell viability was calculated Equation (3).

$$\text{Cell viability} = [(R_A - R_E)/(R_B - R_E)] \times 100\% \quad (3)$$

(R_A, R_B, R_E were defined as the absorbance of the experimental samples, untreated samples and blank controls, respectively).

2.6. Cell viability

For AS1411 analysis, A549 , MCF-7 and K562 cells were seeded into 96-well plates at a density of 3000 cells well $^{-1}$ and grown for 24 h. Then, 200 nM AS1411 and 26 μM DXBA [or GenOpti (Opti-MEM^{TM}) from M&C Gene Technology as control] were added to the culture medium. After 48 h, the cell viability was assayed using the Cell Counting Kit-8 (CCK-8) (Dojindo Laboratories). After incubating the cells with a CCK-8 solution for 1.5 h, the optical density was measured and considered as an evaluation of cytotoxicity.

For G3139 analysis, MCF-7/ADR cells were seeded into 96-well plates at a density of 3000 cells well^{-1} and grown for 24 h. Then, 0–400 nM G3139 and 7.5–15 μM DNCA (or GenOpti as control) were added to the culture medium, and the procedure described for AS1411 analysis was performed.

2.7. Flow cytometry analysis of cellular uptake

For AS1411 analysis, A549 cells were seeded into 6-well plates at a density of 1×10^5 cells well^{-1} and grown for 24 h. The cells were treated with 100 nM FAM-AS1411 and 7.5 μM DNCA (or GenOpti as control) in 10% FBS for 4 h. After that, the cells were harvested by trypsinization and washed with pre-cooled PBS. The cellular uptake was immediately observed on a FACS Calibur flow cytometer (Becton Dickinson, San Jose, CA, USA).

For RNA analysis, A549 cells were seeded into 6-well plates at a density of 3×10^5 cells well^{-1} and grown for 24 h. The cells were treated with 100 nM FAM-RNAs and 10.5 μM DNCA (or GenOpti as control) with or without 10% FBS for 4 h. The other operations performed were same as those in AS1411 analysis.

For pMB3 and pRL-TK analysis, human embryonic kidney 293 (HEK293) cells were seeded into 24-well plates at a density of 5×10^4 cells well^{-1} and grown for 24 h. The cells were treated with 100 ng pMB3, 10 ng pRL-TK and 16.7 μM DNCA, DNTA, DNXA (DNCA:DNTA = 1:1) or Lipofectamine 2000 (1 μL) without 10% FBS for 4 h. FBS was added into the culture after 6 h. The effective acting time of plasmids was only 6 h. Cells were harvested 24 h after transfection and lysed through passive cell lysis (Macgene, China). The fluorescence intensities were determined with 30 μL of cell lysate using the Dual-Luciferase Assay System (Promega).

For pEGFP-N1 analysis, HEK293 cells were seeded into 12-well plates at a density of 1×10^5 cells well^{-1} and grown for 24 h. The

cells were treated with 100 ng pEGFP-N1 and 20 μM DNCA or Lipofectamine 2000 (2 μL) with or without 10% FBS for 4 h. GFP was expressed in the cells, and other operations performed were the same as those in AS1411 analysis.

2.8. CD measurement

The AS1411 (25 μM) and DNCA (0.65 mM) complexes with and without annealing operation or CLD (0.15 mM) complexes with ultrasonic treatment (10 min, r.t.) were dissolved in 1× PBS buffer (138 mM NaCl, 2.7 mM KCl, 10 mM Na_2HPO_4, 1.76 mM KH_2PO_4, pH 7.2–7.4), and analyzed by CD spectroscopy (Jasco J610 spectrometer, Japan) using 0.4-mL quartz cuvettes with a 0.5-mm path length. The measurements of the wavelengths ranged from 230 nm to 400 nm at 25 °C.

2.9. Confocal microscopy

A549 cells were grown on confocal observation dishes for 24 h. Then, 100 nM FAM-labeled AS1411 and 7.5 μM DNCA (or GenOpti from M&C Gene Technology as control) were added to the culture medium. After 4 h, the culture medium was removed, and the cells were fixed in 4% formaldehyde for 15 min and washed twice with PBS. Cells were then stained with Hoechst 33342 (Solarbio) for 10 min and observed under an A1Rsi confocal microscope (Nikon Instruments Inc.). Confocal images were obtained using NIS-Elements software (Nikon Instruments Inc.) and analyzed using ImageJ software.

2.10. Inverted fluorescence microscopy

HEK293 cells were seeded into 12-well plates at a density of 1×10^5 cells $well^{-1}$ and grown for 24 h. The cells were treated with 100 ng pEGFP-N1 and 10–20 μM (7.45–14.9 μg, 1.0 mL) DNCA or Lipofectamine 2000 (1 μg, 1.0 mL) with 10% FBS for 4 h. GFP was expressed in the cells, the culture medium was removed, and the cells were fixed in 4% formaldehyde for 15 min and washed twice with PBS. Cells were observed under an Olympus IX83 microscope and the images were analyzed using ImageJ software.

2.11. Flow cytometry analysis of the cell cycle

A549 cells were plated into 6-well plates at a density of 2×10^5 cells $well^{-1}$ and grown for 24 h. After treatment, cells were harvested by trypsinization and stained with PI using the CycleTEST™ PLUS DNA Reagent Kit (BD Biosciences) following the suggested protocol and analyzed by FACSCalibur™ cytometry (BD Biosciences). The percentage of cells in G1/G0, S and G2/M phases was determined using the ModFit program.

2.12. Apoptosis assay

Cell apoptosis was quantified using an Annexin V-FITC/PI Apoptosis Detection Kit (BD Pharmingen). After treatment, the A549 cells seeded into 6-well plates were harvested, washed with cold PBS twice and resuspended in 100 μL of 1× binding buffer. Next, 5 μL of annexin V-FITC and 5 μL of PI were added to each sample, and the cells were incubated at room temperature for 20 min in the dark. The stained samples were then determined by FACSCalibur™ cytometry (BD Biosciences).

2.13. Pharmacokinetic of DNCA/AS1411 nanoparticles in vivo

4-5-week-old BALB/c-nude mice (female, n = 2) were seeded into A549 cells. When the tumors reached about 200 mm^3, the mice were treated with control, AS1411 and DNCA/AS1411 by peritumoral injection [33]. The images were measured at hour 1, hour 6, day 1, day 2 and day 5. Subsequently, tumors were taken out and measured as well. Concentration of the control, Cy7-AS1411: 0.5 mg kg^{-1}; concentration of DNCA: 3.35 mg kg^{-1}. All animal experiments were carried out according to protocols approved by the Committee for Animal Research of Peking University, China (Authorization No. LA2017194). The operations were conformed to the Guide for the Care and Use of Laboratory Animals (NIH publication No. 86–23, revised 1985).

2.14. Flow cytometry analysis of the endocytotic pathway

HepG2 (3×10^5 per well) cells were cultured in three holes of a six-well plate and allowed to proliferate for 24 h. The inhibitors (genistein 40 μg mL^{-1}; chlorpromazine 5 μg mL^{-1}), which blocked the endocytotic pathway of caveolae-mediated endocytosis and clathrin-mediated endocytosis, respectively, were added into the cells 0.5 h prior to the transfection. Various nanoparticles containing 6-FAM-labeled RNAs at a final concentration of 100 nM were exposed to the cells. After 4 h of incubation, the cells were harvested and centrifuged at 1 g for 3 min. Subsequently, the precipitates were washed with pre-cooled PBS and filtered to achieve a homogeneous distribution in the solution. The cellular uptake was immediately observed on a FACS Calibur flow cytometer (Becton Dickinson, San Jose, CA, USA).

2.15. Preparation of cell lysate

A375 cells were gathered to a centrifuge tube and washed with PBS solution, then lysed in 0.5 mL of buffer containing 10 mM Pipes-NaOH (pH 6.8), 300 mM sucrose, 100 mM NaCl, 1 mM EGTA, 3 mM $MgCl_2$ and 0.5% Triton X-100. Subsequently, the cells were centrifuged at 15,000 g for 20 min at 4 °C, and the liquid supernatants were collected.

2.16. RNA nanoparticle degradation assay with cell lysate

All of the 6-FAM-labeled RNAs (20 pmol) annealed to the DNCA at the base ratio of 5:1. The nanoparticles were added into cell lysate (1 μL, 300 cell μL^{-1}) and incubated in PBS (10 μL) at 37 °C. The samples were removed after the indicated amounts of time and immediately frozen in liquid nitrogen. Following the addition of 6 × RNA loading buffer (2 μL, DingGuo, Beijing, China), the aliquots were analyzed on 20% polyacrylamide gels at 110 V for 120 min.

2.17. Statistical analysis

One-way repeated analysis of variance (ANOVA) measurements were used for the analysis of the experimental data. All data were the average of experimental values, and error bars were used to denote standard deviations. As appropriate, the significant differences were identified using P-values obtained with Student's t-test: n.s. $P > 0.05$; *$P < 0.05$; **$P < 0.01$; ***$P < 0.001$; or ****$P < 0.0001$. All statistical analysis was carried out using GraphPad Prism 6.0 software.

3. Results and discussion

3.1. Characteristics of DXBAs

The morphologies of DXBAs were investigated by TEM analysis. As seen from Fig. 2A, all nucleobase-lipids could self-assemble as spherical vesicles in 1 × phosphate-buffered saline (PBS) buffer. The nanoparticle diameters were approximately 150–220 nm,

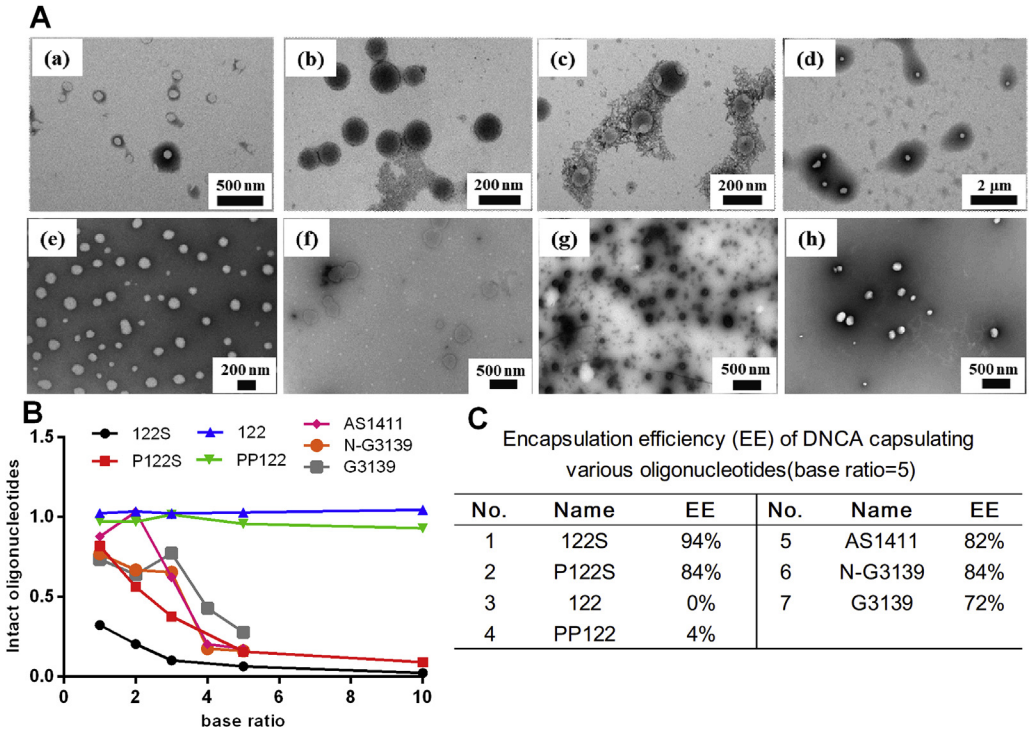

C

Encapsulation efficiency (EE) of DNCA capsulating various oligonucleotides(base ratio=5)

No.	Name	EE	No.	Name	EE
1	122S	94%	5	AS1411	82%
2	P122S	84%	6	N-G3139	84%
3	122	0%	7	G3139	72%
4	PP122	4%			

Fig. 2. A. TEM morphologies of DXBAs and their nanocomplexes with oligonucleotides. (a)–(h) each represented DOTA, DOCA, DNTA, DNCA, DNCA/G3139, DNCA/AS1411, DNCA/122S, DNCA/P122S; B. Gel electrophoresis analysis of intact bands after oligonucleotide annealing to DNCA lipids at different base ratios. The concentration of FAM-labeled RNAs was 2 μM and DNAs were 10 μM. C. Encapsulation efficiency of DNCA in encapsulating oligonucleotides at a base ratio = 5.

which is a suitable parameter for an extended circulation period and application of the lipids *in vivo* [34,35]. Besides, there were no obvious effects on the morphologies when DNCA encapsulated various single-stranded oligonucleotides, which indicated that this lipid had potential for nucleic acids delivery. In addition, it was found that unmodified and peptide-conjugated single-stranded oligonucleotides (including 122S, P122S, AS1411 and N-G3139) could be effectively encapsulated at a base ratio of 5:1 (>80%); however, fully phosphorothioate oligo (G3139) slightly reduced the encapsulation efficiency (72%). Interestingly, the duplexes (122 and PP122) were rarely loaded into DNCA nanoparticle, even if the base ratio increased to 10:1 (Fig. 2B/2C). The results demonstrated that DNCA lipid especially bound to single-stranded oligonucleotides.

3.2. Simulated self-assembly of DXBAs

The morphologies and self-assemblies of DXBAs were simulated using Chem3D and Material Studio 5.5 software, and the supramolecular membrane was measured by the Langmuir method. For DNCA and DOCA (Fig. 3A–B), the surface pressure was significantly enhanced accompanied by trough area reduction within 30–80 cm^2. In contrast to DNTA and DOTA, these cytimidine-based lipids could form more compact structures. It was possible that cytosine possesses a stronger hydrophilia than thymine, resulting in hydrophobic tails relatively perpendicular to the air/water interface with a compact structure (Fig. S2).

In addition, the DXBAs (such as DNCA) were divided into several moieties, represented by beads with different colors. These areas of red, cyan and blue denote the hydrophilic nucleobase head group, linkage and hydrophobic chains, respectively (Fig. S3). As seen in Fig. 3C/3D, DNCA and DNTA could form spherical nanoparticles, wherein the hydrophilic head-group was located on the surface and the lipid chains were tightly inserted into each other due to strong hydrophobic interactions. The results of the self-assembly simulation for DXBAs were consistent with TEM observations.

3.3. Toxicity and transfection efficiency of DXBAs for G-quadruplexes

Guanine-rich (G-rich) DNA and RNA molecules can fold into non-canonical structures stabilized by the stacking of G-quartets, which is widely used in bioanalysis and biomedical applications [36]. Effective endocytosis remains the main barrier for clinical application of AS1411 (G4-aptamer, 26-mer). To the best of our knowledge, AS1411 was rarely individually delivered by lipids as an antitumor agent. The biomolecule was frequently carrier-free [37], alterative used as a targeting molecule on the surface of nanoparticles [38,39].

The cytotoxicity and transfection efficiency were evaluated, respectively. As shown in Fig. 4A, the viability of HeLa cell has remained above 90% after transfection with DXBAs at 65 μM, implying their biocompatiblity. Besides, DNCA/AS1411 nanoparticles showed high anti-proliferative activity (>50%) at a low concentration in both A549 and MCF-7 cells (Fig. 4B), especially in A549/TXL cells (Fig. S4). In addition, the cellular uptake of DNCA/AS1411 nanoparticle was nearly triple than naked AS1411 (Fig. 4C), which demonstrated its high transfection efficiency. Similarly, poly-A or poly-G encapsulated by DNTA or DNCA also exhibited significant cellular uptake improvement (Fig. S5).

Circular dichroism (CD) measurement (Fig. 4D) showed that AS1411 encapsulated by a cationic lipid (CLD) reduced the absorption peak, while DNCA encapsulation (after annealing) induced a higher absorption peak. This indicated that the cationic lipid damaged G-quadruplexes, but DNCA encapsulation was in favor. Additionally, the mixture of DNCA and AS1411 (before annealing) was similar to naked AS1411, which implied that the annealing

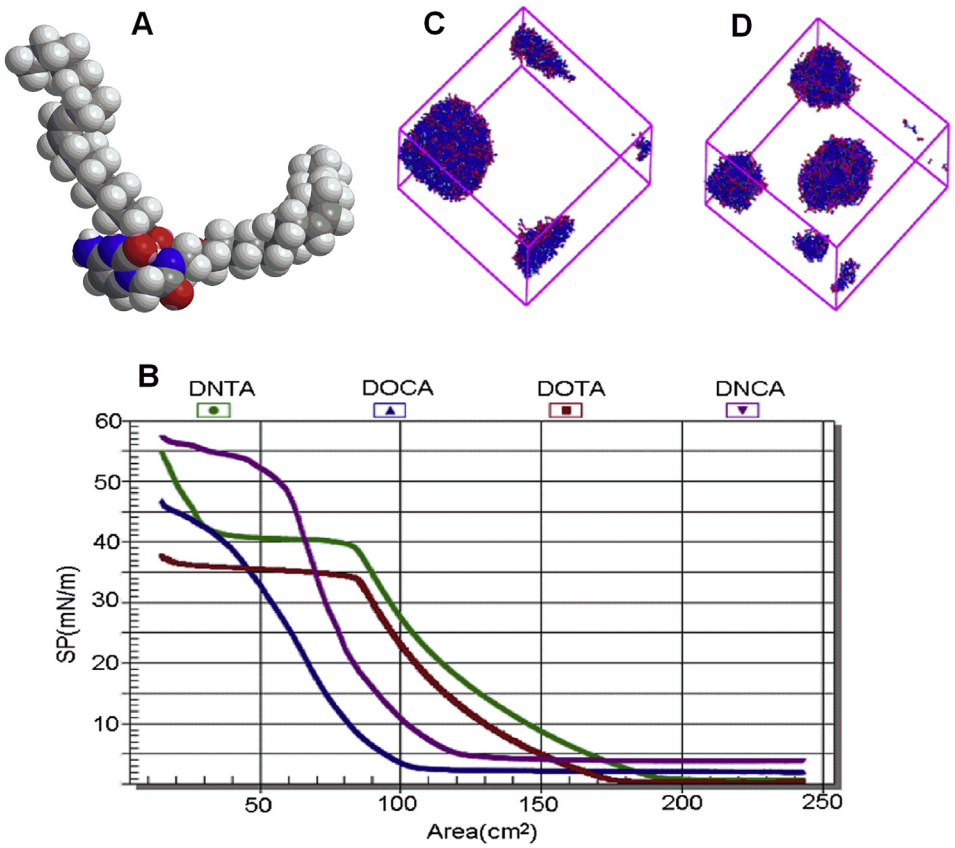

Fig. 3. The supramolecular structure of DXBA. A. The DNCA molecule with minimized energy. B. The surface pressure-molecular area isotherms of DXBA. The X-axis represents trough areas and the Y-axis represents surface pressure. C,D. The self-assembly of DNCA (C) and DNTA (D) in water. The areas of red, cyan and blue denote the hydrophilic nucleobase head group, linkage and hydrophobic chains, respectively. (For interpretation of the references to color in this figure legend, the reader is referred to the Web version of this article.)

strategy played a significant role in interaction. Moreover, the nanoparticles in intracellular conditions (after annealing and lysis) exhibited the best absorption, demonstrating its superiority for biological applications. On the contrary, CD spectra of N-G3139, G3139 and RNA did not show remarkable differences after annealing to DNCA (Fig. S6), which suggested there was a specific interaction between DNCA and G4-aptamers based on π-π interaction.

Confocal microscopy was used to verify the transfection efficiency of DNCA/AS1411. As seen in Fig. 5, the naked AS1411 rarely permeated into the cancer cells (2.24 ± 0.04), while DNCA/AS1411 nanoparticles significantly enhanced transmembrane ability (25.6 ± 6.2). The results were consistent with flow cytometry analysis, indicating the superiority of DNCA as a vehicle for G4-aptamer delivery. Colocalization analysis (Fig. S7A/7B) showed that DNCA/AS1411 could permeate into cells as time prolongs, while the endocytic efficiency of naked AS1411 reached a maximum at 6 h. Besides, the colocalization of nanoparticles and lysosomes (Fig. S7A, C) showed that DNCA/AS1411 rarely fused with lysosomes (Pearson's_Rr ≤ 0), but plenty of naked AS1411s were endocytosed into lysosomes (Pearson's_Rr ≥ 0). The results indicated that the DNCA/AS1411 nanoparticles effectively escaped from lysosomes or avoided lysosome-related endocytosis, which was in favor of their biological exertion.

3.4. Biological property alteration by DNCA/AS1411 nanoparticles

To evaluate the biological alteration of DNCA encapsulation, annexin V-FITC/PI staining flow cytometry was used to assess cell apoptosis. Compared with the control or naked AS1411 (Fig. 6A/6B), DNCA/AS1411 nanoparticles were greater stopped in the S-phase (36%). Besides, the nanocomplex significantly enhanced early apoptosis. All data showed that DNCA was a successful vehicle for AS1411 delivery, and exerted biological activity improvement *in vitro*.

Biodistribution of DNCA/AS1411 nanoparticles were evaluated as well *in vivo*. The BALB/c mice suffering A549 tumors (about 200 mm^3) were administrated with GenOpti, Cy7 labeled AS1411 and DNCA/Cy7-AS1411 by peritumoral injection, respectively. The results showed (Fig. 7A) that extensive AS1411 was metabolized within 1 day (fluorescence intensity$<1.6 \times 10^8$), and DNCA/AS1411 prolonged the duration exceeding 2 days (fluorescence intensity$>2.1 \times 10^8$, Fig. 7B). After 5 days, plenty of DNCA/AS1411 nanoparticles maintained in tumor compared with naked AS1411 (Fig. 7C). In addition, the toxicity examination showed that DNCA/AS1411 had no obvious effect on body weight of nude mice by intravenous injection or peritumoral injection (Fig. S8), suggesting its safety *in vivo*.

3.5. Transfection efficiency of DNCA for RNAs

In further, ss(ds)-RNAs and their peptide-conjugated derivatives were selected for verifying the transfection efficiency of DNCA for RNAs. Flow cytometry (FCM) assay was carried out to evaluate the cellular uptake and endocytic pathway. Lipofectamine 2000 was used as a control for determining the diversity between cationic and DNCA lipids. The results (Fig. 8A–B) showed that naked RNAs

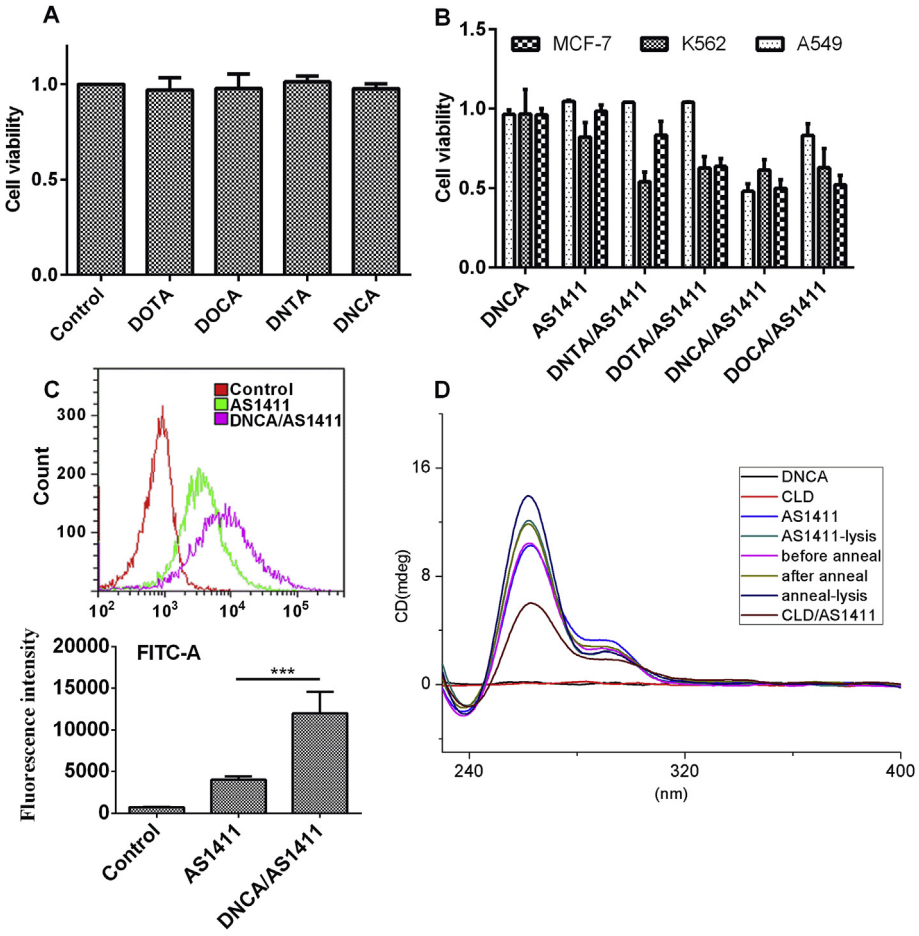

Fig. 4. A. Cytotoxicity test of DXBA in Hela cells over 72 h (DXBA: 65 μM). B. Anti-proliferative activity of AS1411 encapsulated by DXBA on A549, MCF-7 and K562 cells. Cell viability was assayed 48 h after addition of AS1411 using the CCK-8 assay (AS1411: 200 nM; DXBA: 26 μM). C. Cellular uptake of FAM-labeled AS1411 in A549 cells (AS1411: 200 nM; DNCA: 26 μM). D. CD spectrum of AS1411 encapsulated by DNCA in a simulated intracellular environment (AS1411: 25 μM; DNCA: 0.65 mM).

could not permeat the membrane. The cellular uptake of DNCA/RNAs was superior to Lipofectamine 2000/RNAs, especially in 10% FBS culture medium. Additionally, the cellular uptake of ssRNAs was higher than dsRNA, despite of its bad serum stability. It suggested that DNCA lipid tended to bind ssRNA rather than dsRNA. However, DNCA could be used as a helper lipid effectively reduced the dosage of cationic lipid for siRNA delivery [40].

The peptide-conjugation was contributed to regulate delivery pathway for siRNAs [41]. Endocytic pathway analysis (Fig. 8C) showed that peptide-conjugated RNA encapsulated by DNCA (DNCA/P122S) significantly enhanced the caveolin-mediated endocytosis (CvME, $P < 0.0001$). However, the Lipofectamine 2000 encapsulation (Lipo/P122S) did not show a comparable difference in the channel rate. In addition, the RNAs encapsulated by DNCA significantly reduced rate of CvME in comparison with Lipofectamine 2000, which suggested the superiority of DNCA and peptide-conjugation in avoiding lysosome degradation [42–44]. A non-denatured polyacrylamide gel electrophoresis assay was performed to verify the intracellular stability. As Fig. 8D seen, the ssRNAs (DNCA/122S, DNCA/P122S) could be almost completely loaded into the nanoparticles. However, bands appeared immediately once addition of fresh cell lysis (0 m). It indicated that ssRNAs could be released from the nanoparticles in intracellular conditions. The RNAs (122S, P122S) all degraded over 30 min, which indicated that the 3′-peptide conjugation had no obvious effect on ssRNA stability. In addition, DNCA/122S nanoparticles were cleaved within 30 min, while DNCA/P122S nanoparticles exhibited clear electrophoretic bands at the 3 h point. It proved that the peptide-conjugation specifically interacted with DNCA lipid and enhanced the nanoparticle stability.

3.6. Transfection efficiency of DXBAs for antisense oligonucleotides

Antisense oligonucleotide with phosphorothioation (G3139), which was used in clinical trials targeting Bcl-2 mRNA [45–47], was carried out for verifying chemical modification influence. The unmodified oligonucleotide (N-G3139) was as a control. The results (Fig. 9) showed that DNCA/G3139 nanoparticles exhibited better antiproliferation than other lipids (DOCA, DNTA and DOTA) upon A549 or A549/TXL cells. This nanocomplex achieved 35% anticancer suspression at 400 nM (concentration of G3139); however, the antiproliferative activity did not furtherly improve, accompanied by the concentration of DNCA enhancement (7.5–15 μM). The results suggested that G3139 could be delivered by DNCA lipid despite a low level of efficacy. Nevertheless, high transfection efficiency would recover through doping with a slight of CLD in DNCA lipid (n:n, 1:9, data not shown).

3.7. Transfection efficiency of DXBAs for plasmids

Plasmids pMB3, pRL-TK and pEGFP-N1 were used for evaluating transfection efficiency. The pMB3 expresses firefly luciferase, and

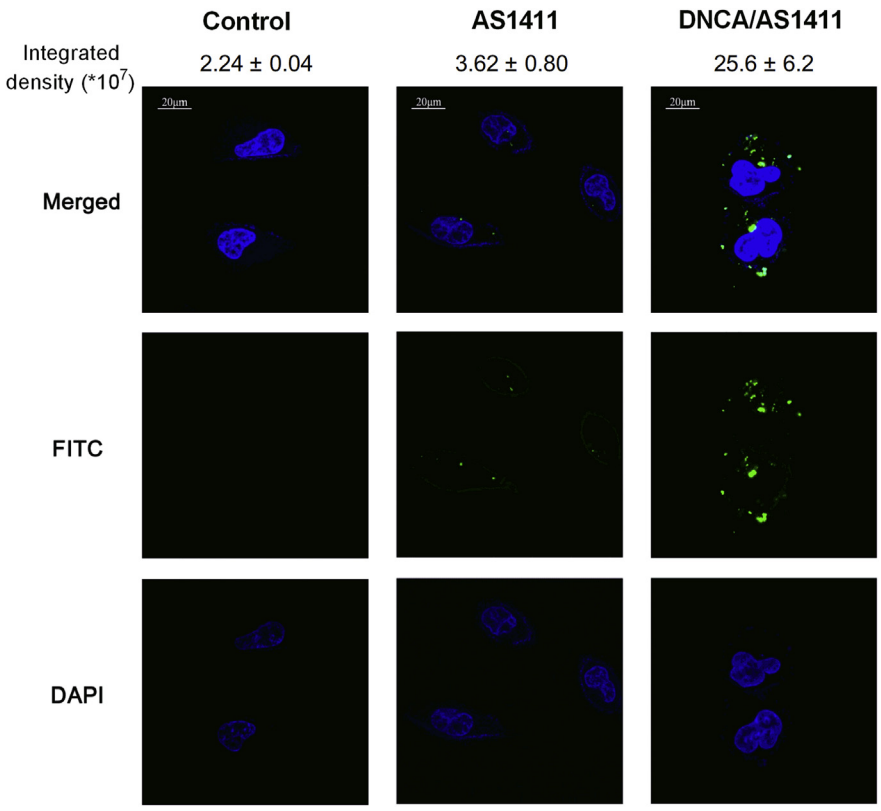

Fig. 5. Confocal microscopy of FAM-AS1411/DNCA nanoparticles over 24 h (FAM-labeled AS1411: 50 nM; DNCA: 6.5 μM). All bars are 20 μm.

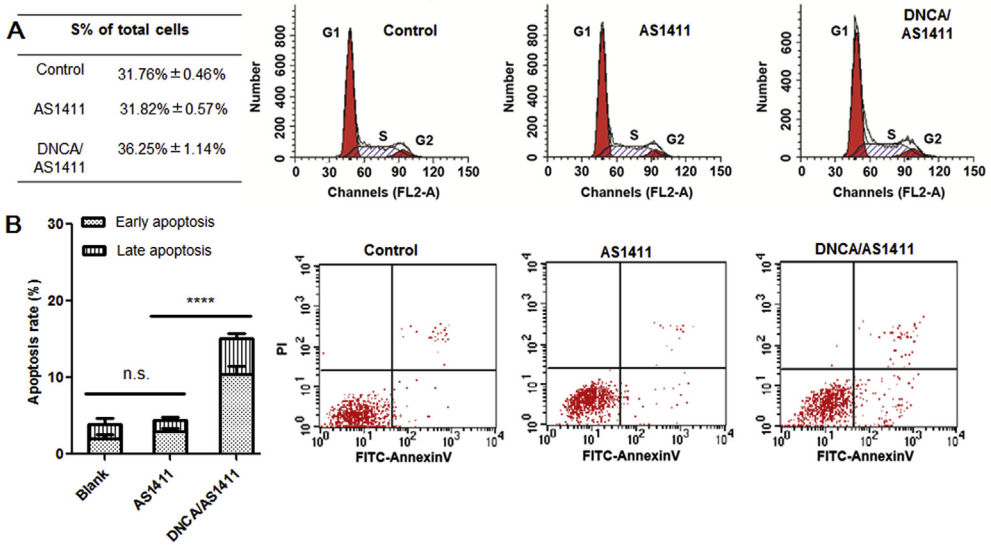

Fig. 6. The cell cycle effects and apoptosis induced by AS1411 (encapsulated by DNCA) in A549 cells. A. The cell cycle tests results. B. The cell apoptosis test. Concentration of the control, AS1411: 100 nM; concentration of DNCA: 7.5 μM.

pRL-TK expresses renilla luciferase [48]. Results (Fig. 10A) showed that both DNCA and DNTA enabled to transfect plasmids, although their transfection efficiency was nearly half that of Lipofectamine 2000 in cell cultures without 10% FBS. Interestingly, when applied in serum conditions, DNCA displayed outstanding characteristics, with transfection efficiency better than that of Lipofectamine 2000 (Fig. 10B). Inverted fluorescence microscopy analysis (Fig. 10C) showed that the transfection efficiency of 10–20 μM DNCA was basically equivalent to that of 1 g L^{-1} Lipofectamine 2000 for pEGFP-N1. This indicated that DNCA has the potential to replace Lipofectamine 2000 for plasmid transfection, such as in the CRISPR/Cas 9 system applied *in vivo*.

4. Conclusions

We reported a novel class of nucleoside-based lipids and

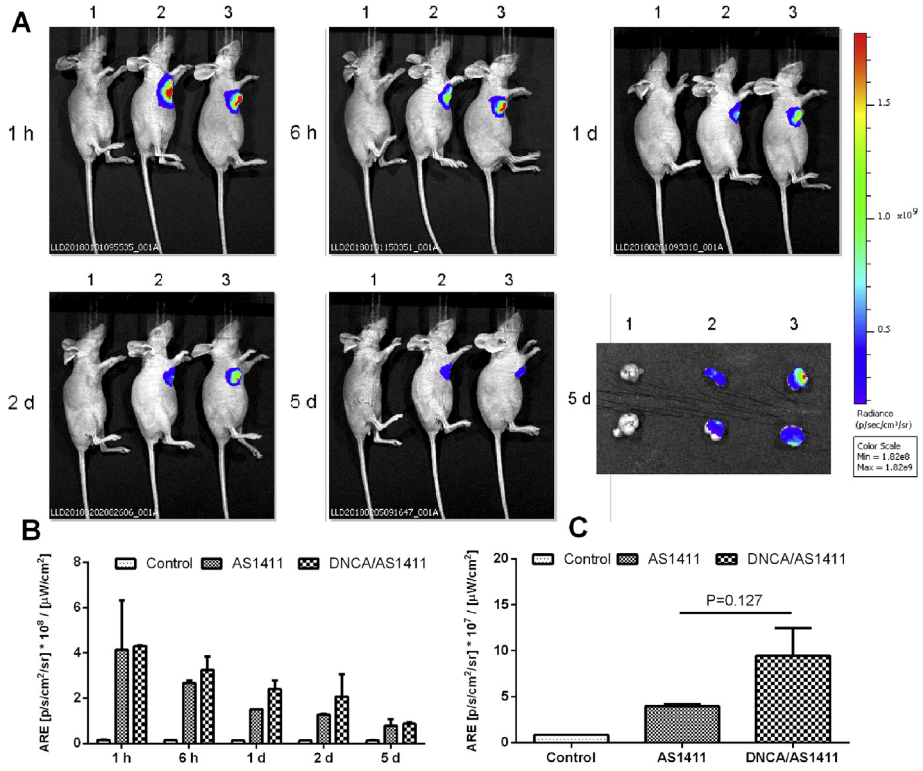

Fig. 7. DNCA/AS1411 nanoparticles *in vivo* imaging. A. Group 1,2,3 represented nude mice (n = 2) treated with Blank, Cy7-AS1411 and DNCA/Cy7-AS1411 complexes, respectively. The images were measured after administration by peritumoral injection at hour 1, hour 6, day 1, day 2 and day 5. Subsequently, tumors were taken out and measured as well. Concentration of the control, Cy7-AS1411: 0.5 mg kg^{-1}; concentration of DNCA: 3.35 mg kg^{-1}. B. Quantified fluorescence data of nude mice treated with Blank, Cy7-AS1411 and DNCA/Cy7-AS1411 complexes, respectively. C. Quantified fluorescence data of tumors after 5 days. (B/C) The Y-axis (ARE) represented Average Radiant Efficiency.

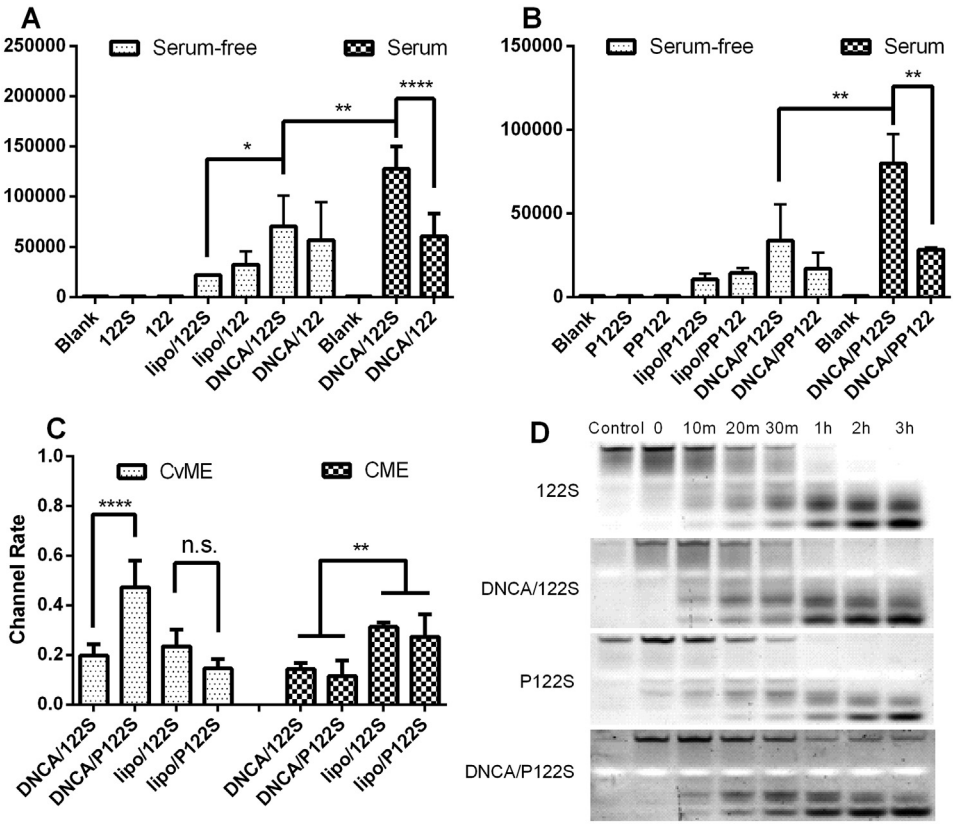

Fig. 8. Cellular uptake and intracellular stability of RNAs (encapsulated by DNCA). (A/B) Flow cytometry assay of the 6′-FAM-labeled RNAs encapsulated by DNCA. A. Unmodified RNAs; B. peptide-conjugated RNAs. C. The channel rate of the RNA nanoparticles penetration into the cellular membrane. D. Electrophoretic bands of 6′-FAM-labeled ssRNAs and complex nanoparticles upon cell lysis. These RNAs (20 pmol) were added into fresh lysate (300 cell μL^{-1}, 1 μL) and incubated for varied periods of time at 37 °C. RNAs without cell lysis treatment were used as control samples to mark the intact RNA band. The base ratio was 5:1.

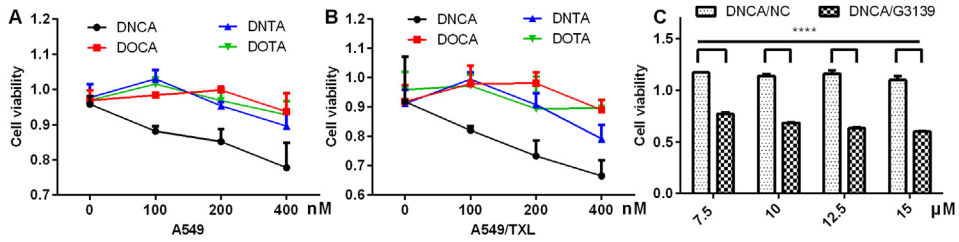

Fig. 9. Anti-proliferative activity of G3139 encapsulated by DXBA in A549 cells (A) and A549/TXL cells (B) (G3139: 100–400 nM; DXBA: 7.5 μM). C. Cell viability with exposure to the NC and to G3139 encapsulated by DNCA in A549/TXL cells. (NC, G3139: 400 nM; DNCA: 7.5–15 μM).

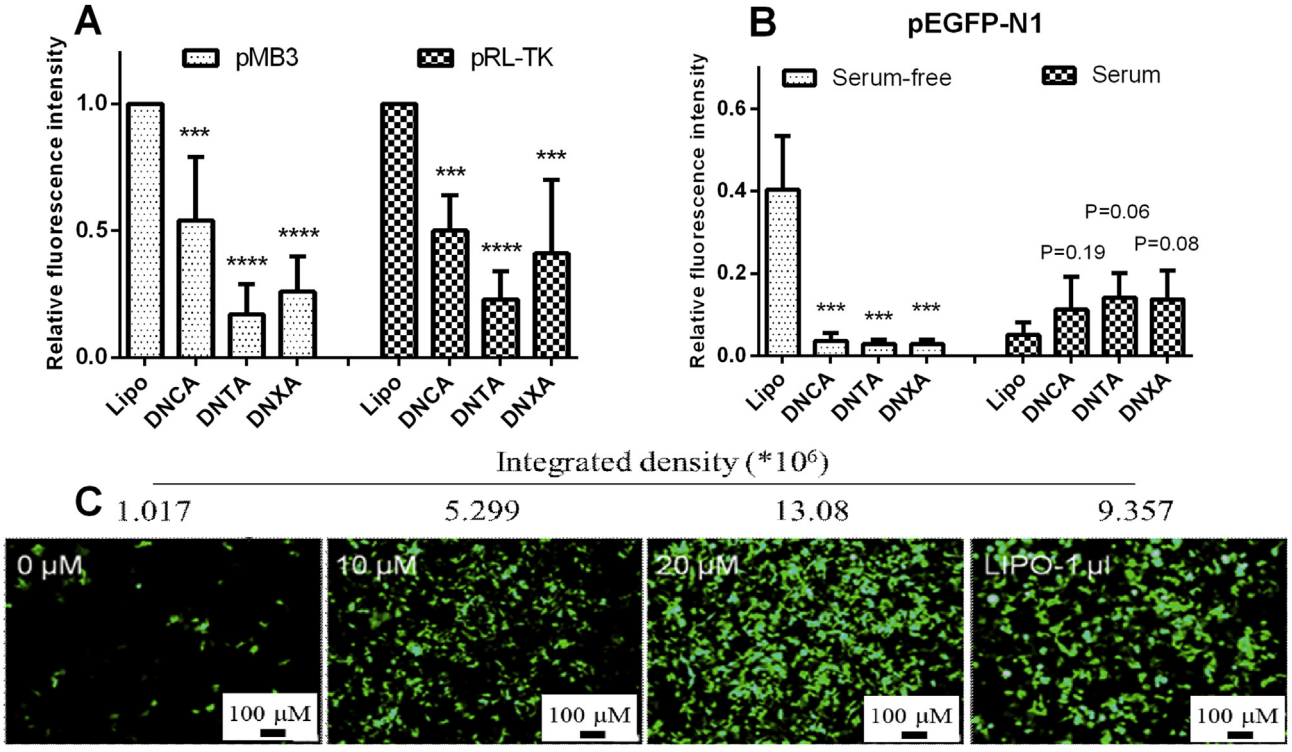

Fig. 10. Plasmid transfection efficiency of DNCA, DNTA and a mixture of both. A. Flow cytometry analysis of pMB3 (100 ng) and pRL-TK plasmid DNA (10 ng) encapsulated by DNCA, DNTA, DNXA (16.7 μM) and Lipofectamine 2000 (1 μL) without FBS; B. Flow cytometry analysis of pEGFP-N1 (100 ng) encapsulated by DNCA, DNTA, DNXA (20 μM) and Lipofectamine 2000 (2 μL) (-: no FBS, +: 10% FBS); C. Inverted fluorescence microscopy of PEGFP-N1 (100 ng) encapsulated by DNCA (0–20 μM) and Lipofectamine 2000 (1 μL). The fluorescence microscopy was performed after 24 h.

systematically evaluated their morphologies and nucleic acid transfection abilities. These lipids efficiently delivered single-stranded oligonucleotides and plasmid DNA in serum medium. The materials significantly regulated the endocytic pathway for RNA entrapment and interacted with peptides to produce compact nanostructures. In particular, the DNCA lipid has perfectly resolved the problem of G4-aptamer (AS1411) encapsulation, delivery and biological exertion. This lipid could induce the formation of AS1411 G4-secondary structures, and released the oligonucleotide in intracellular environment. The DNCA/AS1411 nanoparticles showed preferable biocompatibility *in vitro* and *in vivo*. In addition, they were able to permeate into cancer cells, escape from lysosome degradation, promote apoptosis, regulate the cell cycle *in vitro* and prolong the duration *in vivo*, which led to effective anticancer activity, especially for taxol-resistant cells. DNCA transfection has great potential for use with therapeutic G4-aptamers, as well as in other nucleic acid-based drug applications.

Author contributions

Z.J.Y. conceived the project. Y.M. and Y.J.Z. designed the experiment. Y.J.Z., Y.M., C.W., D.L.P., S.L., M.Y.Y., Z.P.X., X.T.Y., W.T.Z., X.Y.Z., Y.D.L., Y.F.P. J.S., S.H.W. and Z.G. performed the experiments. Y.M. analyzed the data and wrote the manuscript with input from all the authors. L.H.Z and Z.J.Y proposed constructive discussions and supervised the research.

Acknowledgement

We thank the Academy of Military Medical Sciences for technology support with Langmuir trough analysis, and Prof. Yiguang Jin for the help with the surface pressure-molecular area isotherms of DXBA. This work was supported by the Ministry of Science and Technology of China (Grant No. 2017ZX09303013, 2012CB720604) and the National Natural Science Foundation of China (Grant No. 21778006, 21332010).

Appendix A. Supplementary data

Supplementary data related to this article can be found at https://doi.org/10.1016/j.biomaterials.2018.06.012.

References

[1] D. Zhi, Y. Bai, J. Yang, S. Cui, Y. Zhao, H. Chen, S. Zhang, A review on cationic lipids with different linkers for gene delivery, Adv. Colloid Interface Sci. 253 (2018) 117–140.

[2] S.W. Cho, M. Goldberg, S.M. Son, Q. Xu, F. Yang, Y. Mei, S. Bogatyrev, R. Langer, D.G. Anderson, Lipid-like nanoparticles for small interfering RNA delivery to endothelial cells, Adv. Funct. Mater. 19 (19) (2009) 3112–3118.

[3] W. Ngamcherdtrakul, J. Morry, S. Gu, D.J. Castro, S.M. Goodyear, T. Sangvanich, M.M. Reda, R. Lee, S.A. Mihelic, B.L. Beckman, Z. Hu, J.W. Gray, W. Yantasee, Cationic polymer modified mesoporous silica nanoparticles for targeted siRNA delivery to HER^{2+} breast cancer, Adv. Funct. Mater. 25 (18) (2015) 2646–2659.

[4] T. Yang, T. Bantegui, K. Pike, R. Bloom, R. Phipps, S. Bai, In vitro evaluation of optimized liposomes for delivery of small interfering RNA, J. Liposome Res. 24 (4) (2014) 270–279.

[5] M.G. Toscano, J. van der Velden, S. van der Werf, M. Odijk, A. Roque, R.J. Camacho-Garcia, I.G. Herrera-Gomez, I. Mancini, P. de Haan, Generation of a vero-based packaging cell line to produce SV40 gene delivery vectors for use in clinical gene therapy studies, Mol. Ther. Methods Clin. Dev. 6 (2017) 124–134.

[6] I. Villate-Beitia, G. Puras, C. Soto-Sanchez, M. Agirre, E. Ojeda, J. Zarate, E. Fernandez, J.L. Pedraz, Non-viral vectors based on magnetoplexes, lipoplexes and polyplexes for VEGF gene delivery into central nervous system cells, Int. J. Pharm. 521 (1–2) (2017) 130–140.

[7] T.A. Balbino, A.R. Azzoni, L.G. de la Torre, Microfluidic devices for continuous production of pDNA/cationic liposome complexes for gene delivery and vaccine therapy, Colloids Surfaces B Biointerfaces 111 (2013) 203–210.

[8] J.H. Jeong, T.G. Park, S.H. Kim, Self-assembled and nanostructured siRNA delivery systems, Pharm. Res. 28 (9) (2011) 2072–2085.

[9] M.M. Nordling-David, G. Golomb, Gene delivery by liposomes, Isr. J. Chem. 53 (2013) 737–747.

[10] H. Ando, A. Okamoto, M. Yokota, T. Asai, T. Dewa, N. Oku, Polycation liposomes as a vector for potential intracellular delivery of microRNA, J. Gene Med. 15 (10) (2013) 375–383.

[11] S.T. Crooke, R.S. Geary, Clinical pharmacological properties of mipomersen (Kynamro), a second generation antisense inhibitor of apolipoprotein B, Br. J. Clin. Pharmacol. 76 (2) (2013) 269–276.

[12] D. Wu, H. Han, Z. Xing, J. Zhang, L. Li, W. Shi, Q. Li, Ideal and reality: barricade in the delivery of small interfering RNA for cancer therapy, Curr. Pharmaceut. Biotechnol. 17 (3) (2016) 237–247.

[13] K. Jiang, Biotech comes to its 'antisenses' after hard-won drug approval, Nat. Med. 19 (3) (2013), 252–252.

[14] F. Wang, L.S. Qi, Applications of CRISPR genome engineering in cell biology, Trends Cell Biol. 26 (11) (2016) 875–888.

[15] J. Kopecek, Polymer-drug conjugates: origins, progress to date and future directions, Adv. Drug Deliv. Rev. 65 (1) (2013) 49–59.

[16] K. Sanderson, Bioengineering: what to make with DNA origami, Nature 464 (7286) (2010) 158–159.

[17] K.R. Kim, D.R. Kim, T. Lee, J.Y. Yhee, B.S. Kim, I.C. Kwon, D.R. Ahn, Drug delivery by a self-assembled DNA tetrahedron for overcoming drug resistance in breast cancer cells, Chem. Commun. 49 (20) (2013) 2010–2012.

[18] B. Yang, X. Ming, C. Cao, B. Laing, A. Yuan, M.A. Porter, E.A. Hull-Ryde, J. Maddry, M. Suto, W.P. Janzen, R.L. Juliano, High-throughput screening identifies small molecules that enhance the pharmacological effects of oligonucleotides, Nucleic Acids Res. 43 (4) (2015) 1987–1996.

[19] L. Simeone, G. Mangiapia, C. Irace, A. Di Pascale, A. Colonna, O. Ortona, L. De Napoli, D. Montesarchio, L. Paduano, Nucleolipid nanovectors as molecular carriers for potential applications in drug delivery, Mol. Biosyst. 7 (11) (2011) 3075–3086.

[20] O. Shatz, P. Holland, Z. Elazar, A. Simonsen, Complex relations between phospholipids, autophagy, and neutral lipids, Trends Biochem. Sci. 41 (11) (2016) 907–923.

[21] F. Cuomo, A. Ceglie, F. Lopez, Specific interactions between nucleolipid doped liposomes and DNA allow a more efficient polynucleotide condensation, J. Colloid Interface Sci. 365 (1) (2012) 184–190.

[22] A.G. Kohli, P.H. Kierstead, V.J. Venditto, C.L. Walsh, F.C. Szoka, Designer lipids for drug delivery: from heads to tails, J. Contr. Release 190 (2014) 274–287.

[23] C.M. LaManna, H. Lusic, M. Camplo, T.J. McIntosh, P. Barthelemy, M.W. Grinstaff, Charge-reversal lipids, peptide-based lipids, and nucleoside-based lipids for gene delivery, Acc. Chem. Res. 45 (7) (2012) 1026–1038.

[24] A. Gissot, M. Camplo, M.W. Grinstaff, P. Barthelemy, Nucleoside, nucleotide and oligonucleotide based amphiphiles: a successful marriage of nucleic acids with lipids, Org. Biomol. Chem. 6 (8) (2008) 1324–1333.

[25] X. Mulet, T. Kaasgaard, C.E. Conn, L.J. Waddington, D.F. Kennedy, A. Weerawardena, C.J. Drummond, Nanostructured nonionic thymidine nucleolipid self-assembly materials, Langmuir 26 (23) (2010) 18415–18423.

[26] L. Latxague, A. Patwa, E. Amigues, P. Barthelemy, Glycosyl-nucleolipids as new bioinspired amphiphiles, Molecules 18 (10) (2013) 12241–12263.

[27] Y. Jin, F. Yang, L. Du, Nanoassemblies containing a fluorouracil/zidovudine glyceryl prodrug with phospholipase A2-triggered drug release for cancer treatment, Colloids Surfaces B Biointerfaces 112 (2013) 421–428.

[28] S. Khiati, N. Pierre, S. Andriamanarivo, M.W. Grinstaff, N. Arazam, F. Nallet, L. Navailles, P. Barthélémy, Anionic nucleotide-lipids for in vitro DNA transfection, Bioconjugate Chem. 20 (20) (2009) 1765–1772.

[29] C. Ceballos, C.A. Prata, S. Giorgio, F. Garzino, D. Payet, P. Barthelemy, M.W. Grinstaff, M. Camplo, Cationic nucleoside lipids based on a 3-nitropyrrole universal base for siRNA delivery, Bioconjugate Chem. 20 (2) (2009) 193–196.

[30] D. Pan, J. Sun, H. Jin, Y. Li, L. Li, Y. Wu, L. Zhang, Z. Yang, Supramolecular assemblies of novel aminonucleoside phospholipids and their bonding to nucleic acids, Chem. Commun. 51 (3) (2015) 469–472.

[31] H. Zhang, Thin-film hydration followed by extrusion method for liposome preparation, Meth. Mol. Biol. 1522 (2017) 17–22.

[32] Y. Zhao, M. Byshkin, Y. Cong, T. Kawakatsu, L. Guadagno, A. De Nicola, N. Yu, G. Milano, B. Dong, Self-assembly of carbon nanotubes in polymer melts: simulation of structural and electrical behaviour by hybrid particle-field molecular dynamics, Nanoscale 8 (34) (2016) 15538–15552.

[33] J.J. Weber, J.H. Wong, Periareolar or peritumoral injection of isosulfan blue and the effect on the number of sentinel lymph nodes examined, Am. Surg. 83 (1) (2017) 98–102.

[34] Y. Yang, L. Ren, H. Wang, Strategies in the design of gold nanoparticles for intracellular targeting: opportunities and challenges, Ther. Deliv. 8 (10) (2017) 879–897.

[35] F. Danhier, O. Feron, V. Preat, To exploit the tumor microenvironment: passive and active tumor targeting of nanocarriers for anti-cancer drug delivery, J. Contr. Release 148 (2) (2010) 135–146.

[36] J.R. Kanwar, J.S. Shankaranarayanan, S. Gurudevan, R.K. Kanwar, Aptamer-based therapeutics of the past, present and future: from the perspective of eye-related diseases, Drug Discov. Today 19 (9) (2014) 1309–1321.

[37] X. Fan, L. Sun, K. Li, X. Yang, B. Cai, Y. Zhang, Y. Zhu, Y. Ma, Z. Guan, Y. Wu, L. Zhang, Z. Yang, The bioactivity of D-/L-isonucleoside- and 2′-deoxyinosine-incorporated aptamer AS1411s including DNA replication/microRNA expression, Mol. Ther. Nucleic Acids 9 (2017) 218–229.

[38] M.T. Malik, M.G. O'Toole, L.K. Casson, S.D. Thomas, G.T. Bardi, E.M. Reyes-Reyes, C.K. Ng, K.A. Kang, P.J. Bates, AS411-conjugated gold nanospheres and their potential for breast cancer therapy, Oncotarget 6 (26) (2015) 22270–22281.

[39] D. Wang, B. Liu, Y. Ma, C. Wu, Q. Mou, H. Deng, R. Wang, D. Yan, C. Zhang, X. Zhu, A molecular recognition approach to synthesize nucleoside analogue based multifunctional nanoparticles for targeted cancer therapy, J. Am. Chem. Soc. 139 (40) (2017) 14021–14024.

[40] M.Y. Yang, J. Sun, C. Wang, Y.F. Zhang, L.H. Zhang, Z.J. Yang, Transfection of 3',3''-bis-peptide-siRNA conjugate by cationic lipoplexes mixed with a neutral cytosin-1-yl-lipid, J. Chin. Pharmaceut. Sci. 26 (10) (2017) 719–726.

[41] J. Sun, C. Qiu, Y. Diao, W. Wei, H. Jin, Y. Zheng, J. Wang, L. Zhang, Z. Yang, Delivery pathway regulation of 3′,3″-bis-peptide-siRNA conjugate via nanocarrier architecture engineering, Mol. Ther. Nucleic Acids 10 (2018) 75–90.

[42] T.J. Pucadyil, S.L. Schmid, Conserved functions of membrane active GTPases in coated vesicle formation, Science 325 (5945) (2009) 1217–1220.

[43] J. Nguyen, F.C. Szoka, Nucleic acid delivery: the missing pieces of the puzzle? Acc. Chem. Res. 45 (7) (2012) 1153–1162.

[44] R.G. Parton, K. Simons, The multiple faces of caveolae, Nat. Rev. Mol. Cell Biol. 8 (3) (2007) 185–194.

[45] M.H. Shah, K.A. Varker, M. Collamore, J.A. Zwiebel, D. Coit, D. Kelsen, K.Y. Chung, G3139 (Genasense) in patients with advanced merkel cell carcinoma, Am. J. Clin. Oncol. 32 (2) (2009) 174–179.

[46] Y. Loriot, P. Mordant, B.D. Brown, J. Bourhis, J.C. Soria, E. Deutsch, Inhibition of BCL-2 in small cell lung cancer cell lines with oblimersen, an antisense BCL-2 oligodeoxynucleotide (ODN): in vitro and in vivo enhancement of radiation response, Anticancer Res. 30 (10) (2010) 3869–3878.

[47] P.S. Galatin, R.H. Advani, G.A. Fisher, B. Francisco, T. Julian, R. Losa, M.I. Sierra, B.I. Sikic, Phase I trial of oblimersen (Genasense(R)) and gemcitabine in refractory and advanced malignancies, Invest. N. Drugs 29 (5) (2011) 971–977.

[48] Y. Ma, S. Liu, Y. Wang, Y. Zhao, Y. Huang, L. Zhong, Z. Guan, L. Zhang, Z. Yang, Isonucleotide incorporation into middle and terminal siRNA duplexes exhibits high gene silencing efficacy and nuclease resistance, Org. Biomol. Chem. 15 (24) (2017) 5161–5170.